ACS APPLIED MATERIALS & INTERFACES

Research Article

Cite This: ACS Appl. Mater. Interfaces 2020, 12, 1054−1060

www.acsami.org

Ultrasensitive Fiber-Based ZnO Nanowire Network Ultraviolet Photodetector Enabled by the Synergism between Interface and Surface Gating Effects

Leixin Meng,[†,‡,⊥] Gaoda Li,[†,⊥] Xiaoqiang Tian,[†] Suo Bai,[†] Qi Xu,[§] Xiaofeng Jia,[†] Xin Cui,[∥] Yong Qin,*[,†] and Wangsuo Wu[‡]

[†]Institute of Nanoscience and Nanotechnology and [‡]School of Nuclear Science and Technology, Lanzhou University, Lanzhou 730000, China

[§]School of Advanced Materials and Nanotechnology, Xidian University, Xi'an 710071, China

[∥]College of Chemistry and Chemical Engineering, Guangxi University, Guangxi 530004, China

Supporting Information

ABSTRACT: A flexible UV photodetector with a high on/off ratio is extremely important for environmental sensing, optical communication, and flexible optoelectronic devices. In this work, a flexible fiber-based UV photodetector with an ultrahigh on/off ratio is developed by utilizing the synergism between interface and surface gating effects on a ZnO nanowire network structure. The synergism between two gating effects is realized by the interplay between surface band bending and the Fermi level through the nanowire network structure, which is proved through the control experiments between the ZnO micro/nanowire photodetector and micro/nanowire junction photodetector, and the corresponding Kelvin probe force microscopy (KPFM) measurements. The on/off ratio of the fiber-based ZnO nanowire network UV photodetector reaches 1.98×10^8 when illuminated by 1.0 mW cm^{-2} UV light, which is 20 times larger than the largest reported result under the same UV illumination. This new UV sensor also has a high resolution to UV light intensity change in the nW cm^{-2} range. Furthermore, when the fiber-based photodetector is curved, it still shows excellent performance as above. This work gives a new effective route for the development of a high-performance UV photodetector or other optoelectronic detection devices.

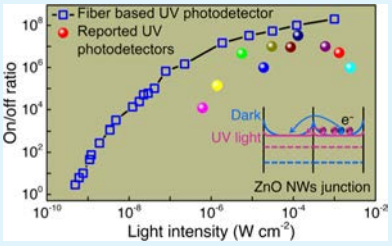

KEYWORDS: *UV photodetectors, synergetic gating effects, ZnO, flexible electronics, on/off ratio*

INTRODUCTION

UV photodetectors have captured increasing attention due to their potential applications in fire monitoring, chemical and biological agent analysis, health monitoring, optical communication, and astronomical exploration.[1−8] Over the past decade, high-on/off-ratio photodetectors are featured with inorganic semiconductor nanomaterials such as nanowires (NWs),[1,2,9−15] nanobelts,[16−20] and nanosheets.[3,21] Benefitting from the large specific surface area of nanomaterials, their channel widths can be modulated through surface gating by absorbed ionized oxygen molecules (O_2^-),[11,13,17] decorated electron extraction materials,[1,14,19,20] or the applied gate voltage.[15,21]

As our previous study reveals, the on/off ratio of the photodetector modulated by surface gating is determined by its dimension:[11,22] semiconductor NW would be completely depleted when its radius is smaller than the depletion width of surface gating, which results to the enlargement of the distance between the Fermi level and conduction band and a dramatic decrease of carrier concentration by several orders of magnitude in the dark. Correspondingly, the on/off ratio is dramatically enhanced by the same orders of magnitude since the photoresponse current is almost not influenced by this process. However, further enhancement of the on/off ratio through surface gating is limited by the interplay of the Fermi level and surface state: adsorption of oxygen molecules or modification of electron extraction materials results into surface states at a constant distance from the surface conduction band, which would extract electrons from the semiconductor when they are below the Fermi level. The complete depletion leads to the enlargement of the distance between the Fermi level and conduction band as well as the decrease of the distance between the Fermi level and surface states, which would eventually reach an equilibrium and prohibit any further depletion.[23] This limitation has been proven by UV photodetectors with various semiconductor materials and extremely small dimension, whereby the largest on/off ratio realized by the surface gating effect is 6 orders of magnitude when the UV intensity is around 1.0 mW cm^{-2}.[22,24−35]

To further improve the on/off ratio, a multinanowire[36,37] or multigrain structure[38−42] is also used, in which the current is

Received: October 7, 2019
Accepted: December 13, 2019
Published: December 13, 2019

DOI: 10.1021/acsami.9b18185
ACS Appl. Mater. Interfaces 2020, 12, 1054−1060

not only modulated by the surface gating effect where the channel width is varied but also by the light-sensitive barrier induced by the absorption and desorption of ambient oxygen molecules at nanowire−nanowire or grain−grain interfaces, i.e., the interface gating effect. The largest on/off ratio of these photodetectors reaches 1×10^7.[39−41] However, the enhancement of the on/off ratio by interface gating is still unclear since the contribution to the on/off ratio from surface and interface gating effects cannot be distinguished experimentally and quantitatively. Correspondingly, the underlying working mechanism of the coupled surface and interface gating effects is still blurred. Decoupling and quantifying the contributions of surface and interface gating effects are consequentially not only vital for the comprehensive understanding of the underlying working mechanism but also essential for taking full advantage of these gating effects to enhance the on/off ratio of UV photodetectors.

In this work, the surface and interface gating effects are first decoupled in the ZnO microwire junction (MW junction) UV photodetector, and it is found that the synergism between these two gating effects could further enhance the on/off ratio. Accordingly, a new kind of the fiber-based ZnO nanowire network (NW network) UV photodetector is designed and developed. It has an ultrahigh on/off ratio of 1.98×10^8 under 1.0 mW cm^{-2} UV light, which is about 20 times larger than the reported largest on/off ratio under UV light with a comparable intensity. What is more, the fiber-based UV photodetector exhibits high flexibility and good resolution to UV light intensity, which makes it applicable for the flexible high-performance UV photodetector or other optoelectronic devices.

RESULTS AND DISCUSSION

ZnO MW Junction UV Photodetector. To decouple the surface and interface gating effects and quantify their respective contributions, the on/off ratio of the ZnO MW junction UV photodetector is first compared with that of the single ZnO MW photodetector. The good crystallinity means that there is no internal grain barrier in ZnO microwires (MWs) (Figure S1). Deposited In/Ag is used as electrodes in both photodetectors. The diameters of ZnO MWs used in both photodetectors are around 10 μm as demonstrated in the insets of Figure 1a,b. ZnO MW junction UV photodetectors were fabricated by overlapping one single-crystal ZnO MW on another to make sure the contact between flat planes of MWs, as shown in Figure 1b and its inset. Due to this contact between MWs, the interface gating effect is introduced and it leads to a dramatic increase of the on/off ratio: under 1.0 mW cm^{-2} UV light illumination, the on/off ratio of the single ZnO MW UV photodetector is 23.5 (Figure 1c), while that of the ZnO MW junction UV photodetector is 2.2×10^6 (Figure 1d). The interface gating effect on the ZnO MW junction results in 0.94×10^5 enhancement of the on/off ratio.

The on/off ratios of MW and MW junction UV photodetectors are modulated by the absorption and desorption processes: in the dark, the depletion of electrons by the absorbed oxygen molecules results in an upward band bending near the surface (surface gating) and an electric barrier across the interface (interface gating). While under UV light illumination, the separation of photogenerated electron−hole pairs by the inner electric field leads to the desorption of oxygen molecules. Hence, the channel width of surface gating widens and the barrier across the interface decreases. Due to the large diameter of ZnO MW compared with the depletion width, the surface gating has a small effect on the carrier concentration of ZnO MW (under UV light, the Fermi level of MW barely moves), which results to a negligible on/off ratio of the ZnO MW UV photodetector (23.5).

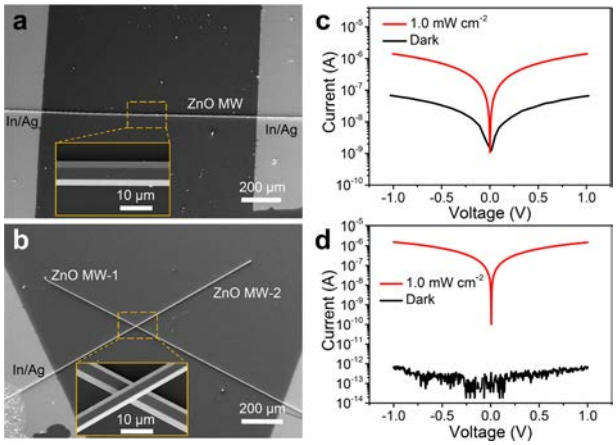

Figure 1. ZnO MW junction UV photodetector and the interface gating effect. (a, b) Scanning electron microscopy (SEM) images of the ZnO MW UV photodetector and ZnO MW junction UV photodetector, respectively. The insets show that the diameters of ZnO MWs are around 10 μm and the flat planes of MWs are overlapped in the ZnO MW junction UV photodetector. The current response of the single ZnO MW UV photodetector (c) is compared with that of the ZnO MW junction UV photodetector (d), which demonstrates that the interface gating effect can lead to a dramatic enhancement of the on/off ratio.

Synergism between Interface and Surface Gating Effects. To further increase the on/off ratio, effective gating on both the interface and surface should be realized. Consequently, a synergism between both gating effects enabled by a NW junction structure is proposed, as shown in Figure 2a. By reducing the diameter of ZnO NW, the complete depletion of NW would result in surface band bending (interface gating by the barrier between NWs) and the enlargement of the distance between the Fermi level and conduction band (surface gating). UV light illumination would result in a decrease of interface barrier height ($\Delta\phi$) and the decrease of the distance between the Fermi level and the conduction band (ΔE).

The equivalent circuit of the NW junction UV photodetector can be simplified as the series of two surface-gated NWs and an interface-gated junction, as shown schematically in Figure 2b. Based on this model, the current density (J) and the on/off ratio of the NW junction UV photodetector (S) can be written as eqs 1 and 2, respectively (see Supporting Information Section 2 for details)

$$J = \sigma \cdot \frac{kT}{eL} \exp\left(-\frac{e\phi}{kT}\right)\left\{\exp\left(\frac{eV_1}{kT}\right) - \exp\left[\frac{e(V_1 - V)}{kT}\right]\right\} \quad (1)$$

$$S = \frac{J_{UV}}{J_{dark}} = \frac{\sigma_{UV}}{\sigma_{dark}} \cdot \exp\left(-\frac{e\Delta\phi}{kT}\right) \quad (2)$$

where J is the current density, σ is the conductivity of ZnO, ϕ is the interface barrier height caused by surface band bending, L is the channel length, V is the applied voltage on the NW junction UV photodetector, V_1 is the voltage drop on the first NW and can be omitted if the applied voltage is small

DOI: 10.1021/acsami.9b18185
ACS Appl. Mater. Interfaces 2020, 12, 1054−1060

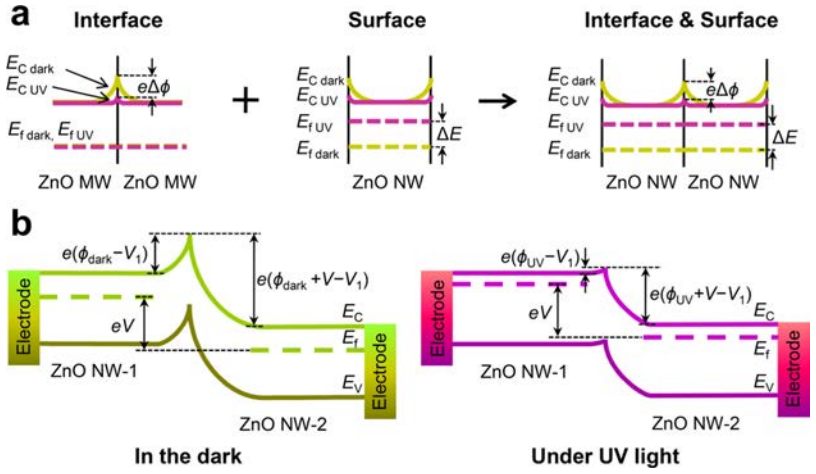

Figure 2. Synergism between interface and gating effects. (a) For the interface gating effect, UV light illumination leads to the decrease of the interface barrier height, while for the surface gating effect on a completely depleted NW, UV light illumination would lead to the decrease of the distance between the Fermi level and conduction band. By utilizing both effects with a NW junction structure, the on/off ratio can be enhanced dramatically. (b) Equivalent circuit of the NW junction can be simplified as the series of two surface-gated NWs and an interface-gated junction, and the voltage across the interface is majorly applied onto the part of the junction at the second NW.

enough,[43] e is the elemental charge, k is the Boltzmann constant, T is the temperature, and $e\Delta\phi = e\phi_{UV} - e\phi_{dark}$ represents the change of the interface barrier height upon illumination with UV light (the subscripts of J, σ, and ϕ denote the corresponding situation, in the dark or under UV light).

In eqs 1 and 2, σ accounts for the current density that is modulated by the distance between the Fermi level and conduction band, i.e., the surface gating effect; $\exp(-e\phi/kT)$ represents the influence of the interface barrier height on the total current density, which is modulated by interface gating. σ and $\exp(-e\phi/kT)$ will increase upon UV light illumination because photoexcited holes will migrate to the surface and lead to the decrease of the surface barrier height and the decrease of distance between the Fermi level and conduction band (right part of Figure 2b).

It should be noted that the distance change between the Fermi level and conduction band and the change of interface barrier height are correlated and that these two parts compose the work function change measured by Kelvin probe force microscopy (KPFM) under UV light illumination (see Supporting Information Section 3 for details). For ZnO MW, the distance change between the Fermi level and conduction band can be omitted as proved by the negligible on/off ratio of the ZnO MW UV photodetector. Consequently, the measured change of work function induced by UV light illumination is attributed to the change of the interface barrier height. As shown in Figure S6, upon illumination of 1.0 mW cm^{-2} UV light, the interface barrier height decreases by 0.34 eV ($e\Delta\phi = -0.34$ eV). Based on eq 2, the on/off ratio of the ZnO MW junction UV photodetector resulted by the interface gating effect would be 4.4×10^5, which is a little larger than the experiment result (0.94×10^5).

This difference is caused by the applied working voltage (V) across the interface, which would result in a decrease of interface barrier height (ϕ_{dark}).[43] In other words, the actual interface barrier height is smaller than the measured one by KPFM since no voltage is applied during KPFM measurement. Consequently, the actual on/off ratio decreases with the increase of working voltage (as verified in Supporting Information Section 5) and a small working voltage across the interface is required to obtain the synergism between interface and surface gating effects. This requirement would be fully investigated in the following sections.

ZnO NW Junction UV Photodetector. To achieve the efficient surface gating effect, the diameter of the ZnO wire must be decreased.[11] Consequently, a new vapor−solid processed chemical vapor deposition is developed to synthesize ZnO NWs with an ultrasmall average diameter of 68 nm, as shown in Figure 3a,b. The crystallinity of ZnO NW is examined by high-resolution transmission electron microscopy (HR-TEM) shown in Figures 3c and S2: the measured interplanar spacing is 0.26−0.28 nm, which corresponds to the d-spacing between (100) lattice planes of hexagonal ZnO. The hexagonal wurtzite structure of ZnO NW is also verified by the

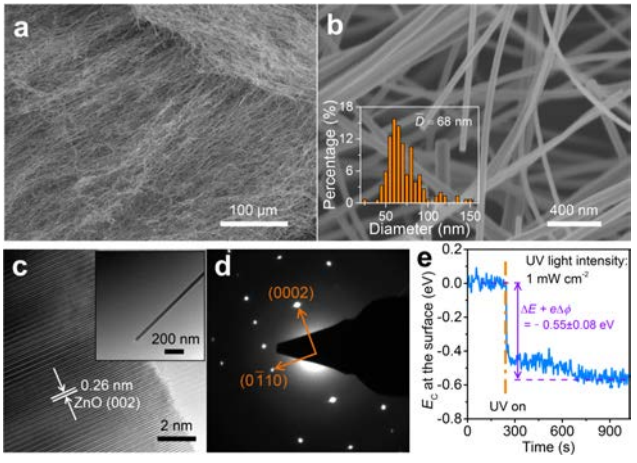

Figure 3. Characterization of ZnO NWs. (a) SEM image of ZnO NWs fabricated by the chemical vapor deposition method. (b) Diameter distribution of ZnO NWs in the SEM image is counted and the average diameter is around 68 nm. (c) In the HR-TEM image of ZnO NW, the interplanar spacing measured is 0.26 nm and corresponds to the d-spacing of (002) lattice planes of hexagonal ZnO. (d) SAED pattern indicates a hexagonal wurtzite structure of ZnO NW. (e) Measured by KPFM and under UV light with 1.0 mW cm^{-2} intensity, the combined change of surface band bending and the distance between the Fermi level and conduction band is 0.55 eV.

DOI: 10.1021/acsami.9b18185
ACS Appl. Mater. Interfaces 2020, 12, 1054−1060

selected area electron diffraction (SAED) pattern shown in Figure 3d and the X-ray diffraction (XRD) spectrum shown in Figure S3. According to these results, the obtained ZnO NWs are single crystalline, which ensures that there is no influence on the on/off ratio from grain boundaries.

Different from the ZnO MW junction UV photodetector, the ultrafine ZnO NW will be completely depleted by the adsorbed ambient oxygen molecules in the dark, which results in surface band bending and the enlargement of the distance between the Fermi level and conduction band, and their combined change ($\Delta E + e\Delta\phi$) is 0.55 eV under UV light illumination with 1.0 mW cm^{-2} intensity as measured by KPFM in Figure 3e. The complete depletion is confirmed by the single ZnO NW UV photodetector (Figure 4a, the inset shows the diameter of NW is around 60 nm), which has a dramatic change of carrier concentration by 4 orders of magnitude under UV light; hence, an on/off ratio of 1.77×10^4 is achieved, as shown in Figure 4b. The change of carrier concentration corresponds to 0.25 eV enlargement of the distance between the Fermi level and conduction band ($\Delta E = E_{UV} - E_{dark}$), as calculated by the formula

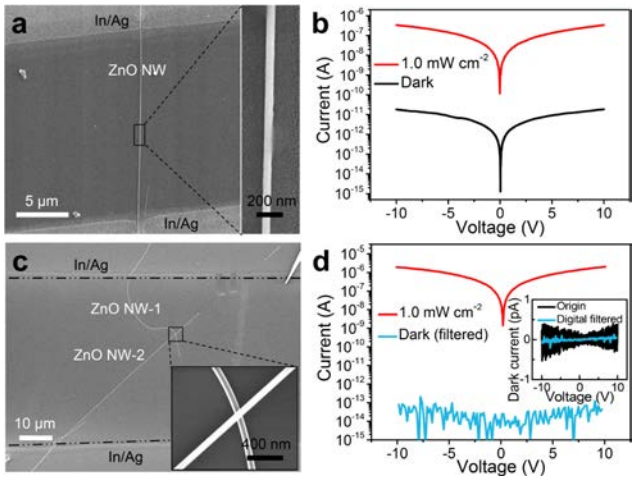

Figure 4. ZnO NW and the NW junction UV photodetector. (a) SEM image of the ZnO NW UV photodetector with In/Ag electrodes. The inset shows that the diameter of NW is around 60 nm. (b) UV response of the ZnO NW photodetector shows an on/off ratio of 1.77×10^4, which results from the surface gating effect. (c) SEM image of the ZnO NW junction UV photodetector. The inset indicates that the diameter of NWs is around 75 nm. (d) On/off ratio of the ZnO NW junction UV photodetector is 4.61×10^7, which is 3 orders of magnitude larger than that of single NW.

$$\frac{\sigma_{UV}}{\sigma_{dark}} = \exp\left(\frac{\Delta E}{kT}\right) \quad (3)$$

where E denotes the distance between the Fermi level and conduction band of bulk. A ZnO NW junction photodetector is also fabricated with two ZnO NWs possessing similar diameters of 75 nm, as shown in Figure 4c and its inset. The on/off ratio of the ZnO NW junction reaches 4.61×10^7, which exhibits an increase by 3 orders of magnitude compared with that of the ZnO NW UV photodetector.

Using the measured $\Delta E + e\Delta\phi$ (0.55 eV) and the calculated ΔE (0.25 eV), the change of interface barrier height, $\Delta\phi$, is deduced as 0.30 eV, which corresponds to 1.08×10^5 times increase in the on/off ratio according to eq 2. Combined with the on/off ratio (1.77×10^4) of the single ZnO NW UV photodetector only influenced by the surface gating effect, the theoretical on/off ratio of the ZnO NW junction UV photodetector could reach 9 orders of magnitude. However, the experimental on/off ratio of the ZnO NW junction UV photodetector reaches only 4.61×10^7, which is 2 orders of magnitude smaller than the theoretical one. As explained in the previous section, the full realization of the synergism between interface and surface gating effects is obstructed due to the large working voltage across the ZnO NW junction interface. A small working voltage across interface and a detectable current are required to obtain a UV photodetector with the high on/off ratio maintained.

Flexible Fiber-Based ZnO NW Network UV Photodetector. To fulfill the above requirements, the ZnO NW network structure is a promising way: the small working voltage across interfaces is realized since the applied voltage (V) across the whole structure is separated by the high number of NW junctions, as illustrated in Figure 5a, and the current across is detectable due to the large number of parallel connections between ZnO NWs. Furthermore, to ensure the flexibility of the UV photodetector, a fiber-based ZnO NW network structure is designed and fabricated, as shown in Figure 5b. NWs are wrapped around and along the Kevlar fiber, forming a network of NW junctions, as demonstrated in the enlarged part of Figure 5b.

The response of the ZnO NW network UV photodetector is shown in Figure 5c. The insert $I-V$ curves show good linear behavior both in the dark and under UV illumination, which is the result of a small voltage approximation at the junctions (see Supporting Information Section 2). The dark current is only 1.14×10^{-14} A at 10 V, indicating effective surface and interface gating effects. Under illumination of 1.0 mW cm^{-2} UV light, the current at 10 V reaches 2.30×10^{-6} A, exhibiting an ultrahigh on/off ratio of 1.98×10^8 at 1.0 mW cm^{-2} UV light, which is close to the theoretical prediction (9 orders of magnitude).

The response of the ZnO NW network UV photodetector to UV light with different intensities is measured, as shown in Figure 5d. The photodetector shows a large response range to the light intensity from 0.5 nW cm^{-2} to 1.0 mW cm^{-2}, and even under UV light with intensity as low as 0.5 nW cm^{-2}, the ZnO NW network UV photodetector still exhibits distinct performance (on/off ratio, 3). Compared with other reported photodetectors with high sensitivities, the fiber-based ZnO NW network UV photodetector possesses the highest on/off ratio, under UV light with the same intensity, as shown in Figure 5e.[41,44−49] Typically, for 1.0 mW cm^{-2} UV light, the on/off ratio of the ZnO NW network UV photodetector is 20 times larger than the highest reported on/off ratio.[44] This ZnO NW network UV photodetector also exhibits high resolution to UV light intensity: from 26 to 55 nW cm^{-2}, the small intensity changes by around 3 nW cm^{-2} lead to distinct photocurrent changes, which is essential for its accurate measurement of the UV light intensity in the nW cm^{-2} range.

For flexible electronic devices, the flexibility is quite important for their applications. So, the fiber-based ZnO NW network UV photodetector is tested under the curved condition. The structure itself of the fiber-based ZnO NW network is capable of curving in a large degree and curvature (Figure S11). Under the curved condition, the performance of the ZnO NW network UV photodetector under different UV light intensities is shown in Figure 6a. When the UV light

DOI: 10.1021/acsami.9b18185
ACS Appl. Mater. Interfaces 2020, 12, 1054−1060

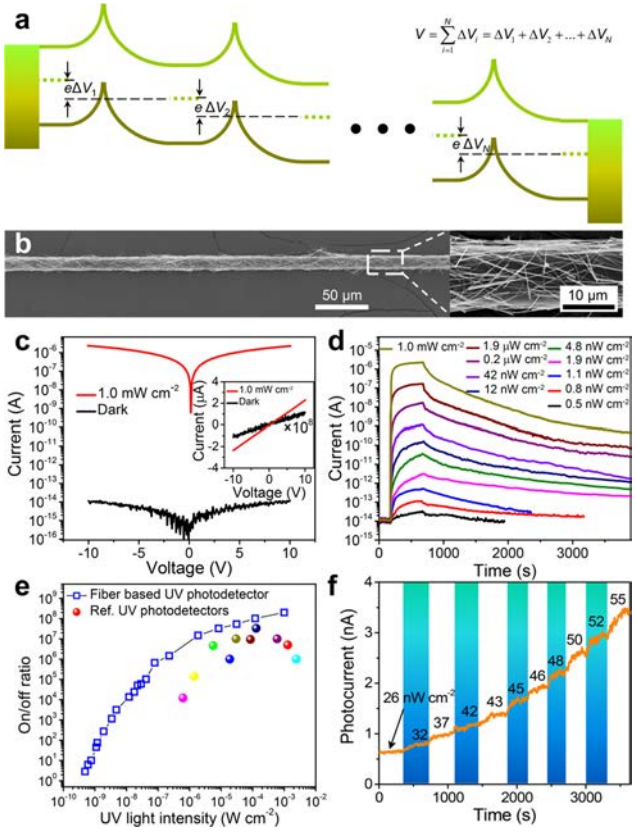

Figure 5. Fiber-based ZnO NW network UV photodetector. (a) Band diagram of the fiber-based ZnO NW network UV photodetector indicates that the applied voltage across the whole structure is separated by the high number of NW junctions as the inset equation shows and a small voltage across each interface is ensured. (b) SEM image of the fiber-based ZnO NW network. The enlarged part indicates that NWs are wrapped around and along the Kevlar fiber and form a network structure. (c) Response to 1.0 mW cm^{-2} UV light. The inset indicates good linear behavior both in the dark and under UV illumination. (d) Response to UV light with different intensities from 0.5 nW cm^{-2} to 1.0 mW cm^{-2}. (e) Comparisons between the on/off ratio of this work (blue square) and reported highest values (circles) under different UV light intensities.[41,44−49] (f) Small change in the UV light intensity leads to a distinct response current that exhibits the good resolution of this photodetector to the intensity of UV light.

intensity changes from 1.1 nW cm^{-2} to 1.0 mW cm^{-2}, the on/off ratio of the ZnO NW network UV photodetector varies from 14 to 0.92 × 10^8, both similar to that of uncurved. The relationship between the on/off ratio and UV light intensity of the curved ZnO NW network UV photodetector is shown in Figure 6b, which also exhibits a similar relationship as that of uncurved. The curved photodetector is shown in the inset of Figure 6b.

The high resolution to the UV light intensity is also reserved under the curved condition: from 0.26 to 2.48 μW cm^{-2}, the intensity change of around 0.2 μW cm^{-2} results into distinct photocurrents, which enable the measurement of the UV light intensity in the μW cm^{-2} range. Furthermore, good repeatability of the ZnO NW network UV photodetector is obtained, as shown in Figure 6d: during six repeated response cycles (repeated dark and UV light illumination conditions), the detected photocurrent differences are within 0.55%, which guarantees the accuracy of UV light detection. What is more,

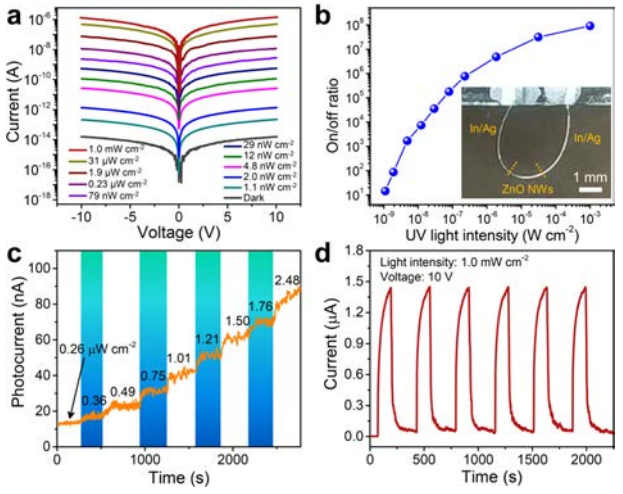

Figure 6. Flexibility and its influence on the ZnO NW junction UV photodetector. (a) UV and dark currents under the curved condition. (b) Relationship between the on/off ratio and UV light intensity of the curved ZnO NW network UV photodetector indicates a similar relationship between the on/off ratio and UV intensity as that of uncurved. The inset is the curved UV photodetector. (c) Resolution of the curved UV photodetector to UV light with different intensities. (d) Repeatability and fast response of the fiber-based ZnO NW network UV photodetector.

quick response and recovery times are also exhibited, 21.5 and 10.5 s, respectively, under 1.0 mW cm^{-2} UV light intensity. These distinctive performances, i.e., an ultrahigh on/off ratio, good flexibility, high resolution to the UV light intensity, and fast response time, make the fiber-based ZnO NW network UV photodetector highly promising for flexible high-performance UV photodetectors or other optoelectronic devices.

CONCLUSIONS

In conclusion, an ultrahigh on/off ratio, high resolution to UV light intensity within different ranges, and structural flexibility are realized by the fiber-based ZnO NW network UV photodetector. Modulated by the surface adsorption of oxygen molecules and the NW network structure, a synergism between interface and surface gating effects is realized by the interplay among the Fermi level, conduction band, and surface band bending. The contributions to the on/off ratio by surface and interface gating effects are evaluated by the ZnO MW or ZnO NW UV photodetector and the corresponding KPFM measurement. This fiber-based NW network gives a new technical route for flexible highly sensitive UV photodetectors and optoelectronic devices.

METHODS

Synthesis of ZnO Microwires (MWs) and Nanowires (NWs). ZnO MWs and NWs were synthesized simultaneously using a chemical vapor deposition (CVD) method through a vapor−solid process. A similar method to synthesize ZnO MWs was reported in our previous work.[50] First, 2.0 g of ZnO powder and 0.4 g of graphite powder were ground in an agate mortar to obtain a uniform mixture. The obtained mixture was put into an alumina boat and placed at the center of a furnace tube. Then, 240 standard-state cubic centimeters per minute (sccm) inert argon and 12 sccm oxygen were introduced into the furnace tube. Afterward, the furnace was heated to 1150 °C for 40 min and then to 1250 °C for 40 min. ZnO MWs grown on the edge of the alumina boat and ZnO NWs grown near the outlet of the furnace tube were obtained.

DOI: 10.1021/acsami.9b18185
ACS Appl. Mater. Interfaces 2020, 12, 1054−1060

KPFM Measurement. We conducted Kelvin probe force microscopy (KPFM) measurement on ZnO MWs and NWs to deduce the amount of the surface barrier height modulated by UV light. The measurements were conducted on an atomic force microscope (Dimension Icon, Bruker) using amplitude modulation mode and an MESP probe (Co/Cr coated). The ZnO MWs were fixed on conductive carbon tape. ZnO NWs were dispersed in ethanol (analytically pure) and drop-casted on heavily doped Si wafer with Au and Cr films presputtered onto it. The surface potentials under UV light were measured under the illumination of a UV LED (λ_{center} = 365 nm) (see Supporting Information Sections 3 and 4 for details).

Fabrication of ZnO MW Junction and NW Junction UV Photodetectors. Two ZnO MWs were transferred onto a clean quartz plate and crossed with each other under optical microscopy. After one end of each MW was fixed by carbon paste, a shadow mask was used to ensure only the fixed ends were exposed and In/Ag electrodes were deposited on the fixed ends by RF magnetron sputtering (In, 3 min and 100 W; Ag, 3 min and 100 W). For the ZnO NW junction UV photodetector, ZnO NWs dispersed in ethanol were dropped on the substrate (silicon slice with a 285 nm SiO_2 surface layer) and after the evaporation of ethanol ZnO NWs would be attached on the substrate by van der Waals force. Two crossed NWs were selected under optical microscopy. A polystyrene (PS) mask was used, and In/Ag electrodes were sputtered on one end of each NW.

Fabrication of the ZnO NW Network UV Photodetector. First, ZnO NWs were dispersed into ethanol with a mass fraction of 0.3%. Then, the ZnO−ethanol dispersion was dropped onto a glass slice and a Kevlar fiber (15 μm diameter) was placed 0.3 mm above the slice, as shown in Figure S9. With the evaporation of ethanol, some of the ZnO NWs were attached around the fiber by van der Waals force (Figure S10).

UV Response Measurement. The currents of UV photodetectors were measured with a femtoammeter (Keysight B2985A). Voltages were provided by a functional generator (DS345). UV lights were provided by a xenon lamp with a band pass filter (309−597 nm) and a 1/4m monochromator (74125, Oriel Instruments). UV intensities were quantified with a silicon photodetector (71675_71580, Oriel Instruments).

■ ASSOCIATED CONTENT

Supporting Information

The Supporting Information is available free of charge at https://pubs.acs.org/doi/10.1021/acsami.9b18185.

Experimental methods and additional explanations: characterization of ZnO microwires (MWs) and nanowires (NWs); calculation of the current across a MW−MW or NW−NW junction; KPFM detection of ZnO MW's surface barrier height change induced by UV light illumination; surface barrier height changes of ZnO NW due to UV illumination; decrease of interface barrier height with the increase of applied voltage; and fabrication of the fiber-based ZnO nanowire network UV photodetector (PDF)

■ AUTHOR INFORMATION

Corresponding Author

*E-mail: qinyong@lzu.edu.cn.

ORCID

Leixin Meng: 0000-0003-4279-9861

Qi Xu: 0000-0003-0546-5360

Yong Qin: 0000-0002-6713-480X

Author Contributions

⊥The manuscript was written through the contributions of all authors. All authors have approved the final version of the manuscript. L.M. and G.L. contributed equally to this work.

Notes

The authors declare no competing financial interest.

■ ACKNOWLEDGMENTS

We sincerely acknowledge the support from the Joint Fund of Equipment Pre-research and Ministry of Education (No. 6141A02022518), the National Program for Support of Top-notch Young Professionals, the Fundamental Research Funds for the Central Universities (No. lzujbky-2018-ot04), NSFC (No. 81702095), and a project funded by the China Postdoctoral Science Foundation (No. 2019M663854).

■ REFERENCES

(1) Li, L.; Gu, L.; Lou, Z.; Fan, Z.; Shen, G. ZnO Quantum Dot Decorated Zn_2SnO_4 Nanowire Heterojunction Photodetectors with Drastic Performance Enhancement and Flexible Ultraviolet Image Sensors. *ACS Nano* **2017**, *11*, 4067−4076.

(2) Zhou, X.; Zhang, Q.; Gan, L.; Li, X.; Li, H.; Zhang, Y.; Golberg, D.; Zhai, T. High Performance Solar-Blind Deep Ultraviolet Photodetector Based on Individual Single-Crystalline Zn_2GeO_4 Nanowire. *Adv. Funct. Mater.* **2016**, *26*, 704−712.

(3) Chu, J.; Wang, F.; Yin, L.; Lei, L.; Yan, C.; Wang, F.; Wen, Y.; Wang, Z.; Jiang, C.; Feng, L.; Xiong, J.; Li, Y.; He, J. High-Performance Ultraviolet Photodetector Based on a Few-Layered 2D $NiPS_3$ Nanosheet. *Adv. Funct. Mater.* **2017**, *27*, No. 1701342.

(4) Amorín, R.; Fontana, A.; Pérez-Montero, E.; Castellano, M.; Guaita, L.; Grazian, A.; Le Fèvre, O.; Ribeiro, B.; Schaerer, D.; Tasca, L. A. M.; Thomas, R.; Bardelli, S.; Cassarà, L.; Cassata, P.; Cimatti, A.; Contini, T.; de Barros, S.; Garilli, B.; Giavalisco, M.; Hathi, N.; Koekemoer, A.; Le Brun, V.; Lemaux, B. C.; Maccagni, D.; Pentericci, L.; Pforr, J.; Talia, M.; Tresse, L.; Vanzella, E.; Vergani, D.; Zamorani, G.; Zucca, E.; Merlin, E. Analogs of Primeval Galaxies Two Billion Years after the Big Bang. *Nat. Astron.* **2017**, *1*, No. 0052.

(5) Peng, M.; Liu, Y.; Yu, A.; Zhang, Y.; Liu, C.; Liu, J.; Wu, W.; Zhang, K.; Shi, X.; Kou, J.; Zhai, J.; Wang, Z. L. Flexible Self-Powered GaN Ultraviolet Photoswitch with Piezo-Phototronic Effect Enhanced On/Off Ratio. *ACS Nano* **2016**, *10*, 1572−1579.

(6) Guo, F.; Yang, B.; Yuan, Y.; Xiao, Z.; Dong, Q.; Bi, Y.; Huang, J. A Nanocomposite Ultraviolet Photodetector Based on Interfacial Trap-Controlled Charge Injection. *Nat. Nanotechnol.* **2012**, *7*, 798−802.

(7) Chen, M.; Zhao, B.; Hu, G.; Fang, X.; Wang, H.; Wang, L.; Luo, J.; Han, X.; Wang, X.; Pan, C.; Wang, Z. L. Piezo-Phototronic Effect Modulated Deep UV Photodetector Based on ZnO-Ga_2O_3 Heterojunction Microwire. *Adv. Funct. Mater.* **2018**, *28*, No. 1706379.

(8) Xu, X.; Chen, J.; Cai, S.; Long, Z.; Zhang, Y.; Su, L.; He, S.; Tang, C.; Liu, P.; Peng, H.; Fang, X. A Real-Time Wearable UV-Radiation Monitor Based on a High-Performance p-CuZnS/n-TiO_2 Photodetector. *Adv. Mater.* **2018**, *30*, No. 1803165.

(9) Cheng, L.; Zheng, Y.; Xu, Q.; Qin, Y. A Light Sensitive Nanogenerator for Self-Powered UV Detection with Two Measuring Ranges. *Adv. Opt. Mater.* **2016**, *5*, No. 1600623.

(10) Bai, S.; Wu, W. W.; Qin, Y.; Cui, N. Y.; Bayerl, D. J.; Wang, X. D. High-Performance Integrated ZnO Nanowire UV Sensors on Rigid and Flexible Substrates. *Adv. Funct. Mater.* **2011**, *21*, 4464−4469.

(11) Li, G.; Meng, L.; Zhu, X.; Gao, W.; Qin, Y.; Chen, L. Clarifying the High On/Off Ratio Mechanism of Nanowire UV Photodetector by Characterizing Surface Barrier Height. *Nanoscale* **2018**, *10*, 2242−2248.

(12) Zheng, W.; Huang, F.; Zheng, R.; Wu, H. Low-Dimensional Structure Vacuum-Ultraviolet-Sensitive (Lambda <200 nm) Photodetector with Fast-Response Speed Based on High-Quality AlN Micro/Nanowire. *Adv. Mater.* **2015**, *27*, 3921−3927.

(13) Soci, C.; Zhang, A.; Xiang, B.; Dayeh, S. A.; Aplin, D. P. R.; Park, J.; Bao, X. Y.; Lo, Y. H.; Wang, D. ZnO Nanowire UV Photodetectors with High Internal Gain. *Nano Lett.* **2007**, *7*, 1003−1009.

(14) Liu, K.; Sakurai, M.; Liao, M.; Aono, M. Giant Improvement of the Performance of ZnO Nanowire Photodetectors by Au Nanoparticles. *J. Phys. Chem. C* **2010**, *114*, 19835−19839.
(15) Kim, W.; Chu, K. S. ZnO Nanowire Field-Effect Transistor as a UV Photodetector; Optimization for Maximum Sensitivity. *Phys. Status Solidi A* **2009**, *206*, 179−182.
(16) Hu, L.; Yan, J.; Liao, M.; Xiang, H.; Gong, X.; Zhang, L.; Fang, X. An Optimized Ultraviolet-A Light Photodetector with Wide-Range Photoresponse Based on ZnS/ZnO Biaxial Nanobelt. *Adv. Mater.* **2012**, *24*, 2305−2309.
(17) Li, L.; Lee, P. S.; Yan, C.; Zhai, T.; Fang, X.; Liao, M.; Koide, Y.; Bando, Y.; Golberg, D. Ultrahigh-Performance Solar-Blind Photodetectors Based on Individual Single-Crystalline $In_2Ge_2O_7$ Nanobelts. *Adv. Mater.* **2010**, *22*, 5145−5149.
(18) Fang, X.; Bando, Y.; Liao, M.; Zhai, T.; Gautam, U. K.; Li, L.; Koide, Y.; Golberg, D. An Efficient Way to Assemble ZnS Nanobelts as Ultraviolet-Light Sensors with Enhanced Photocurrent and Stability. *Adv. Funct. Mater.* **2010**, *20*, 500−508.
(19) Lao, C. S.; Park, M.-C.; Kuang, Q.; Deng, Y.; Sood, A. K.; Polla, D. L.; Wang, Z. L. Giant Enhancement in UV Response of ZnO Nanobelts by Polymer Surface-Functionalization. *J. Am. Chem. Soc.* **2007**, *129*, 12096−12097.
(20) Lao, C.; Li, Y.; Wong, C. P.; Wang, Z. L. Enhancing the Electrical and Optoelectronic Performance of Nanobelt Devices by Molecular Surface Functionalization. *Nano Lett.* **2007**, *7*, 1323−1328.
(21) Zhou, X.; Zhang, Q.; Gan, L.; Li, H.; Zhai, T. Large-Size Growth of Ultrathin SnS_2 Nanosheets and High Performance for Phototransistors. *Adv. Funct. Mater.* **2016**, *26*, 4405−4413.
(22) Xu, Q.; Cheng, L.; Meng, L.; Wang, Z.; Bai, S.; Tian, X.; Jia, X.; Qin, Y. Flexible Self-Powered ZnO Film UV Sensor with a High Response. *ACS Appl. Mater. Interfaces* **2019**, *11*, 26127−26133.
(23) Li, G.; Sun, Z.; Zhang, D.; Xu, Q.; Meng, L.; Qin, Y. Mechanism of Sensitivity Enhancement of a ZnO Nanofilm Gas Sensor by UV Light Illumination. *ACS Sens.* **2019**, *4*, 1577−1585.
(24) Kind, H.; Yan, H.; Messer, B.; Law, M.; Yang, P. Nanowire Ultraviolet Photodetectors and Optical Switches. *Adv. Mater.* **2002**, *14*, 158−160.
(25) Kumar, R. R.; Rao, K. N.; Rajanna, K.; Phani, A. R. Low Temperature Growth of SnO_2 Nanowires by Electron Beam Evaporation and Their Application in UV Light Detection. *Mater. Res. Bull.* **2013**, *48*, 1545−1552.
(26) González-Posada, F.; Songmuang, R.; Den, H. M.; Monroy, E. Room-Temperature Photodetection Dynamics of Single GaN Nanowires. *Nano Lett.* **2012**, *12*, 172−176.
(27) Hu, L.; Yan, J.; Liao, M.; Wu, L.; Fang, X. Ultrahigh External Quantum Efficiency from Thin SnO_2 Nanowire Ultraviolet Photodetectors. *Small* **2011**, *7*, 1012−1017.
(28) Heo, Y.-W.; Pearton, S. J.; Norton, D. P. Size-Dependent UV Photosensitivity of Indium Zinc Oxide. *J. Nanoelectron. Optoelectron.* **2010**, *5*, 143−146.
(29) Li, Q. H.; Gao, T.; Wang, Y. G.; Wang, T. H. Adsorption and Desorption of Oxygen Probed from ZnO Nanowire Films by Photocurrent Measurements. *Appl. Phys. Lett.* **2005**, *86*, No. 123117.
(30) Heo, Y. W.; Kang, B. S.; Tien, L. C.; Norton, D. P.; Ren, F.; La Roche, J. R.; Pearton, S. J. UV Photoresponse of Single ZnO Nanowires. *Appl. Phys. A: Mater. Sci. Process.* **2005**, *80*, 497−499.
(31) Calarco, R.; Marso, M.; Richter, T.; Aykanat, A. I.; Meijers, R.; Hart, A. vd.; Stoica, T.; Lüth, H. Size-Dependent Photoconductivity in MBE-Grown GaN-Nanowires. *Nano Lett.* **2005**, *5*, 981−984.
(32) Han, S.; Jin, W.; Zhang, D.; Tang, T.; Li, C.; Liu, X.; Liu, Z.; Lei, B.; Zhou, C. Photoconduction Studies on GaN Nanowire Transistors under UV and Polarized UV Illumination. *Chem. Phys. Lett.* **2004**, *389*, 176−180.
(33) Fan, Z.; Chang, P.-c.; Lu, J. G.; Walter, E. C.; Penner, R. M.; Lin, C.-h.; Lee, H. P. Photoluminescence and Polarized Photodetection of Single ZnO Nanowires. *Appl. Phys. Lett.* **2004**, *85*, 6128−6130.
(34) Zhang, D.; Li, C.; Han, S.; Liu, X.; Tang, T.; Jin, W.; Zhou, C. Ultraviolet Photodetection Properties of Indium Oxide Nanowires. *Appl. Phys. A: Mater. Sci. Process.* **2003**, *77*, 163−166.
(35) Liu, Z.; Zhang, D.; Han, S.; Li, C.; Tang, T.; Jin, W.; Liu, X.; Lei, B.; Zhou, C. Laser Ablation Synthesis and Electron Transport Studies of Tin Oxide Nanowires. *Adv. Mater.* **2003**, *15*, 1754−1757.
(36) Gedamu, D.; Paulowicz, I.; Kaps, S.; Lupan, O.; Wille, S.; Haidarschin, G.; Mishra, Y. K.; Adelung, R. Rapid Fabrication Technique for Interpenetrated ZnO Nanotetrapod Networks for Fast UV Sensors. *Adv. Mater.* **2013**, *26*, 1541−1550.
(37) Deng, K.; Lu, H.; Shi, Z.; Liu, Q.; Li, L. Flexible Three-Dimensional SnO_2 Nanowire Arrays: Atomic Layer Deposition-Assisted Synthesis, Excellent Photodetectors, and Field Emitters. *ACS Appl. Mater. Interfaces* **2013**, *5*, 7845−7851.
(38) Nasiri, N.; Jin, D.; Tricoli, A. Nanoarchitechtonics of Visible-Blind Ultraviolet Photodetector Materials: Critical Features and Nano-Microfabrication. *Adv. Opt. Mater.* **2019**, *7*, No. 1800580.
(39) Nasiri, N.; Bo, R.; Fu, L.; Tricoli, A. Three-Dimensional Nano-Heterojunction Networks: A Highly Performing Structure for Fast Visible-Blind UV Photodetectors. *Nanoscale* **2017**, *9*, 2059−2067.
(40) Bo, R.; Nasiri, N.; Chen, H.; Caputo, D.; Fu, L.; Tricoli, A. Low-Voltage High-Performance UV Photodetectors: An Interplay between Grain Boundaries and Debye Length. *ACS Appl. Mater. Interfaces* **2017**, *9*, 2606−2615.
(41) Nasiri, N.; Bo, R.; Chen, H.; White, T. P.; Fu, L.; Tricoli, A. Structural Engineering of Nano-Grain Boundaries for Low-Voltage UV-Photodetectors with Gigantic Photo- to Dark-Current Ratios. *Adv. Opt. Mater.* **2016**, *4*, 1787−1795.
(42) Nasiri, N.; Bo, R.; Wang, F.; Fu, L.; Tricoli, A. Ultraporous Electron-Depleted ZnO Nanoparticle Networks for Highly Sensitive Portable Visible-Blind UV Photodetectors. *Adv. Mater.* **2015**, *27*, 4336−4343.
(43) Pike, G. E.; Seager, C. H. The DC Voltage Dependence of Semiconductor Grain-Boundary Resistance. *J. Appl. Phys.* **1979**, *50*, 3414−3422.
(44) Fan, M.-M.; Liu, K.-W.; Chen, X.; Zhang, Z.-Z.; Li, B.-H.; Zhao, H.-F.; Shen, D.-Z. Realization of Cubic ZnMgO Photodetectors for UVB Applications. *J. Mater. Chem. C* **2015**, *3*, 313−317.
(45) Tyagi, M.; Tomar, M.; Gupta, V. Fabrication of an Efficient GLAD-Assisted p-NiO Nanorod/n-ZnO Thin Film Heterojunction UV Photodiode. *J. Mater. Chem. C* **2014**, *2*, 2387−2393.
(46) Kim, D.; Shin, G.; Yoon, J.; Jang, D.; Lee, S.-J.; Zi, G.; Ha, J. S. High Performance Stretchable UV Sensor Arrays of SnO_2 Nanowires. *Nanotechnology* **2013**, *24*, No. 315502.
(47) Dai, Z.; Wei, L.; Xu, D.; Zhang, Y. Ultraviolet Photoresponse of ZnO Nanowire Thin-Film Transistors. *Phys. E* **2012**, *44*, 1999−2004.
(48) Lee, W.-J.; Hon, M.-H. An Ultraviolet Photo-Detector Based on TiO_2/Water Solid-Liquid Heterojunction. *Appl. Phys. Lett.* **2011**, *99*, No. 251102.
(49) Kim, K. H.; Bae, S. Y.; Kim, Y. S.; Hur, J. A.; Hoang, M. H.; Lee, T. W.; Cho, M. J.; Kim, Y.; Kim, M.; Jin, J.-I.; Kim, S.-J.; Lee, K.; Lee, S. J.; Choi, D. H. Highly Photosensitive J-Aggregated Single-Crystalline Organic Transistors. *Adv. Mater.* **2011**, *23*, 3095−3099.
(50) Meng, L.; Xu, Q.; Sun, Z.; Li, G.; Bai, S.; Wang, Z.; Qin, Y. Enhancing the Performance of Room Temperature ZnO Microwire Gas Sensor Through a Combined Technology of Surface Etching and UV Illumination. *Mater. Lett.* **2018**, *212*, 296−298.

DOI: 10.1021/acsami.9b18185
ACS Appl. Mater. Interfaces 2020, 12, 1054−1060